Journal of
Materials Chemistry A

Materials for energy and sustainability

www.rsc.org/MaterialsA

ROYAL SOCIETY
OF CHEMISTRY
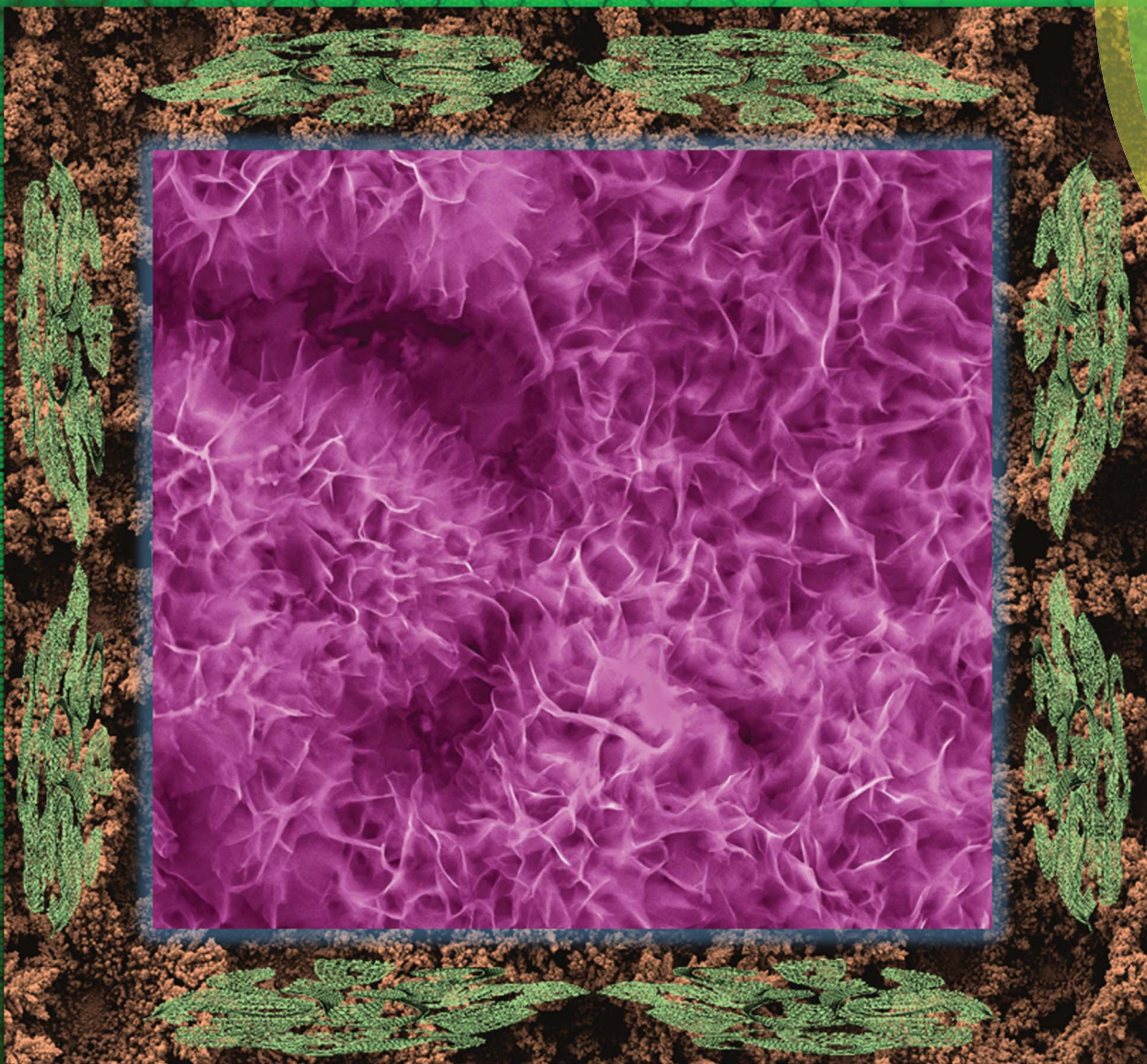
PAPER

Approaching the theoretical capacitance of graphene through copper foam integrated three-dimensional graphene networks†

Ramendra Sundar Dey,[a] Hans Aage Hjuler[b] and Qijin Chi*[a]

We report a facile and low-cost approach for the preparation of all-in-one supercapacitor electrodes using copper foam (CuF) integrated three-dimensional (3D) reduced graphene oxide (rGO) networks. The binder-free 3DrGO@CuF electrodes are capable of delivering high specific capacitance approaching the theoretical capacitance of graphene and exhibiting high charge–discharge cycling stability.

As a new carbon allotrope, graphene holds promise for the development of electrochemical double layer (EDL) capacitors, due to its large specific surface area (with a theoretical specific surface area of 2630 m^2 g^{-1}), high conductivity, chemical stability, low-cost and feasibility of large-scale production.[1] Moreover, the high mechanical strength and flexibility of this atomically thin two-dimensional carbon allotrope makes graphene particularly conspicuous to fabricate light, flexible and binder-free supercapacitors.[1a,2] Even though graphene possesses these advantages, graphene-based supercapacitors still have not reached a theoretical capacitance as high as ~550 F g^{-1} due to self-aggregation or re-stacking of graphene sheets.[3] Doping graphene with electroactive capacitive materials (*e.g.* MnO_2, RuO_2, Co_3O_4, polyaniline) enables the construction of pseudo-supercapacitors with high specific capacitances (200–1000 F g^{-1}).[4] On the other hand, inefficient ionic and electronic transport of pseudo-capacitive material-based electrodes often causes specific capacitance fading rapidly over charge–discharge cycling, particularly at high charging–discharging speeds. This is a major setback for the use of graphene-based materials in supercapacitors.[5] Recently, 3D graphene networks have been studied as a possible solution.[3,6] However, most studies have shown that specific capacitance is not as high as expected or high specific capacitance is achieved only with charge–discharge at low current densities (<1 A g^{-1}) or at low potential scan rates (<50 mV s^{-1}). A major cause is attributed to significant π–π re-stacking of graphene sheets during material preparation, assembly and charge–discharge processes, leading to insufficient pore size for access of electrolytes.[7] Therefore, it is highly desirable to develop a

binder-free, self-supported integrated system for construction of 3D porous graphene based high-performance super-capacitors. The present work is motivated towards such a goal.

The two major technical challenges (or limitations) in the use of 3DrGO materials for supercapacitors are: (1) 3DrGO is mechanically fragile and its electrical conductivity is practically low, and (2) attachment (or transfer) of 3DrGO networks to a current collector with *low contact resistance* and *without destroying 3D structures* is another considerable challenge. The latter would be of crucial limitation in the practical use of 3DrGO-based materials for supercapacitors, even if they possess a large specific surface area. This work has demonstrated a facile and low-cost strategy to prepare 3DrGO on copper foam (CuF), with the aim at the cost-effective fabrication of all-in-one supercapacitor electrodes with large effective contact areas and high cycling performances, leading to approach the theoretical capacitance of graphene. Recently, there have been some reports related to Cu supported graphene material based supercapacitor electrodes, but their performances need to be further improved.[8] To the best of our knowledge, this is the first attempt using CuF as both a template for assembly of 3DrGO and a current collector for supercapacitors. The resulting binder-free supercapacitor electrodes show substantial energy density and high cycling stability.

The overall procedure for the preparation of 3DrGO on CuF is illustrated schematically in Scheme 1. Digital photos of resulting electrode materials obtained at different stages are shown in the bottom row in Scheme 1 and Fig. S1 ESI.† Electrochemical reduction was performed to convert self-assembled GO to rGO (Fig. S2 ESI†). The morphology and structures of the rGO@CuF hybrid material were characterized systematically by field-emission gun scanning electron microscopy (FEG-SEM) and AFM. The surface structure of the Cu foil before and after the deposition of CuF was imaged by FEG-SEM, and the representative images are compared in Fig. S3 (ESI†). Fig. 1 shows typical SEM images of 3DrGO@CuF hybrid materials deposited

[a]Department of Chemistry, Technical University of Denmark, DK-2800 Kongens Lyngby, Denmark. E-mail: cq@kemi.dtu.dk; Fax: +45 45883136; Tel: +45 45252032
[b]Danish Power Systems, Dreyersvej 30, 2960 Rungsted Kyst, Denmark
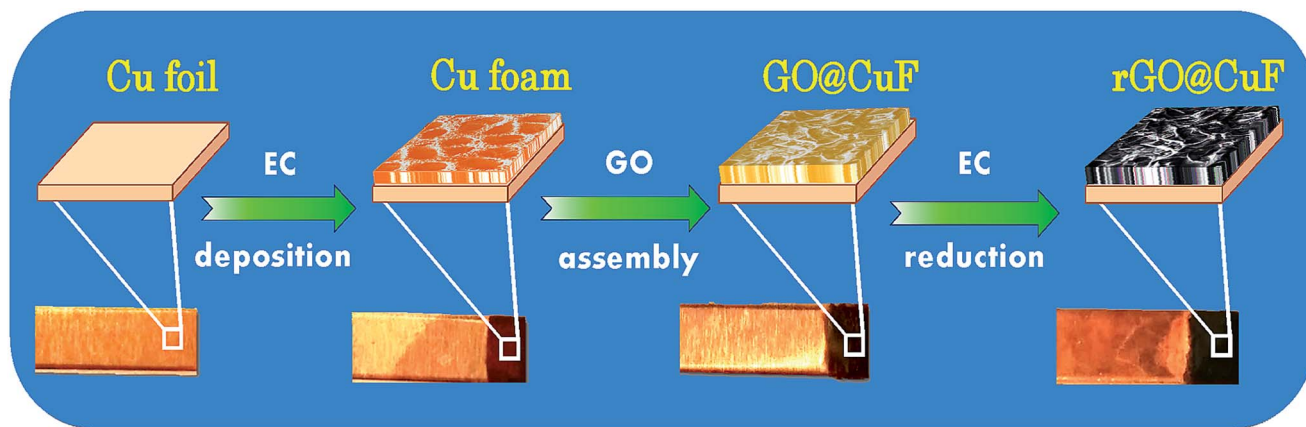
Scheme 1 Schematic representation of the overall procedure for the stepwise fabrication of 3DrGO@CuF electrode materials. Digital pictures of the resulting electrode materials at different stages are shown in the bottom row.

on CuF, by which three types of structures in different locations are clearly revealed. Fig. 1a–c show the structure of 3DrGO on the boundary of CuF, which is the porous graphene network consisting of interconnected nanosheets. Fig. 1d–f show the structure of the 3DrGO inside the CuF pore, and Fig. 1g–i show the structure of 3DrGO at the wall of the CuF pore. High-resolution SEM images (Fig. 1c, f and i) suggest that the attachment of GO sheets does not change the frame structure of CuF but GO nanosheets self-assemble into hierarchically porous structures using CuF as the template and support. The detailed structures of 3DrGO@CuF clearly show that the material possesses a large effective contact area. The partial overlapping (or linking) of rGO sheets leads to the formation of a 3D porous network. The interconnection is driven most likely by different types of interactions between graphene nanosheets, including van der Waals attraction, hydrogen bonding *via* oxygen-containing groups at the sheet edges and partial π–π stacking.[9]

It is noticed that the structure of 3DrGO is also dependent on the CuF pore size, thickness and the GO loading amount. We have prepared Cu foams with various pore sizes ranging from 80 to 120 μm by changing the electrodeposition time (Fig. S4 ESI†). The average size of pores in CuF is determined from the size-distribution histograms (Fig. S5 ESI†). The thickness of the CuFs prepared with an electrodeposition time of 40, 50 and 60 s is 100, 125 and 150 μm, respectively (Fig. S4c, f and i ESI†). The Cu foams with a pore size of ≈120 μm (Fig. S6 ESI†) show the best suitability for self-assembly of GO nanosheets to form high-performance 3DrGO networks. It is clear from Fig. S7 (ESI†) that 0.08 mg cm^{-2} is the optimized loading amount for GO to form porous networks which fully covered the CuF but without visible stacking. The increased amount of GO results in aggregation and blocks the porous structure of both 3DrGO and CuF (Fig. S7c–e ESI†).

AFM was used to further disclose the structural features of 3DrGO@CuF samples. High-resolution AFM images enable to offer more details of the structural features. Similar to SEM observations, AFM *first* reveals that rGO sheets maintain 3D network structures of CuF throughout all prepared samples and are partially stacked in some regions interconnected to form the

3D framework (Fig. 2a–d). More details also revealed that rGO sheets are crumpled and tightly cover CuF pores over the whole surface of CuF (Fig. 2a and b). This observation suggests that there is strong adhesion between rGO sheets and the Cu substrate. It is also noted that similar AFM images of GO@CuF (Fig. S8 ESI†) and rGO@CuF (Fig. 2a and b) demonstrate that the 3D structural integrity is not altered by electrochemical reduction. The real surface areas of the 3DrGO@CuF material were measured by an electrochemical approach generally used for porous metal electrodes.[10] We used a popular voltammetry approach to estimate the effective surface areas of the 3DrGO@CuF materials (see ESI†) and is found to be approximately 1000 m^2 g^{-1} (Fig. S9 ESI†).

GO@CuF and rGO@CuF hybrid materials were analyzed by X-ray diffraction (XRD) (Fig. S10 ESI†). The XRD patterns reveal that the typical diffraction peak of GO at $2\theta = 9.1°$ disappears in rGO@CuF samples due to removal of oxygen-containing functional groups from GO planes by electrochemical reduction. Furthermore, the graphite diffraction peak is not observed for rGO@CuF, a clear indication that electrochemical reduction did not cause re-stacking of rGO sheets into graphite. This observation is consistent with those obtained from AFM and SEM images, *i.e.* the overall 3D network structures are retained after electrochemical reduction.[11]

As the material is highly porous, thin, conductive and possess good electrical contact interfaces, 3DrGO@CuF is a promising material for supercapacitor electrodes. The potential of this material for supercapacitors has been tested systematically by the so-called best-practice methods using cyclic voltammetry and galvanostatic charge–discharge measurements. Fig. 3a shows a cyclic voltammogram (CV) of rGO@CuF electrodes at a scan rate of 0.1 V s^{-1}. Rectangular-like, horizontal, largely symmetric features in the CV indicate that rGO@CuF electrodes have ideal EDL capacitive nature and good charge propagation in a potential window of −0.2 V to −0.8 V. Large capacitive currents result from the high specific area of rGO@CuF electrodes and high conductivity. The CVs obtained at different scan rates are compared (Fig. S11 ESI†). With increasing scan rate, the capacitive current increases but the
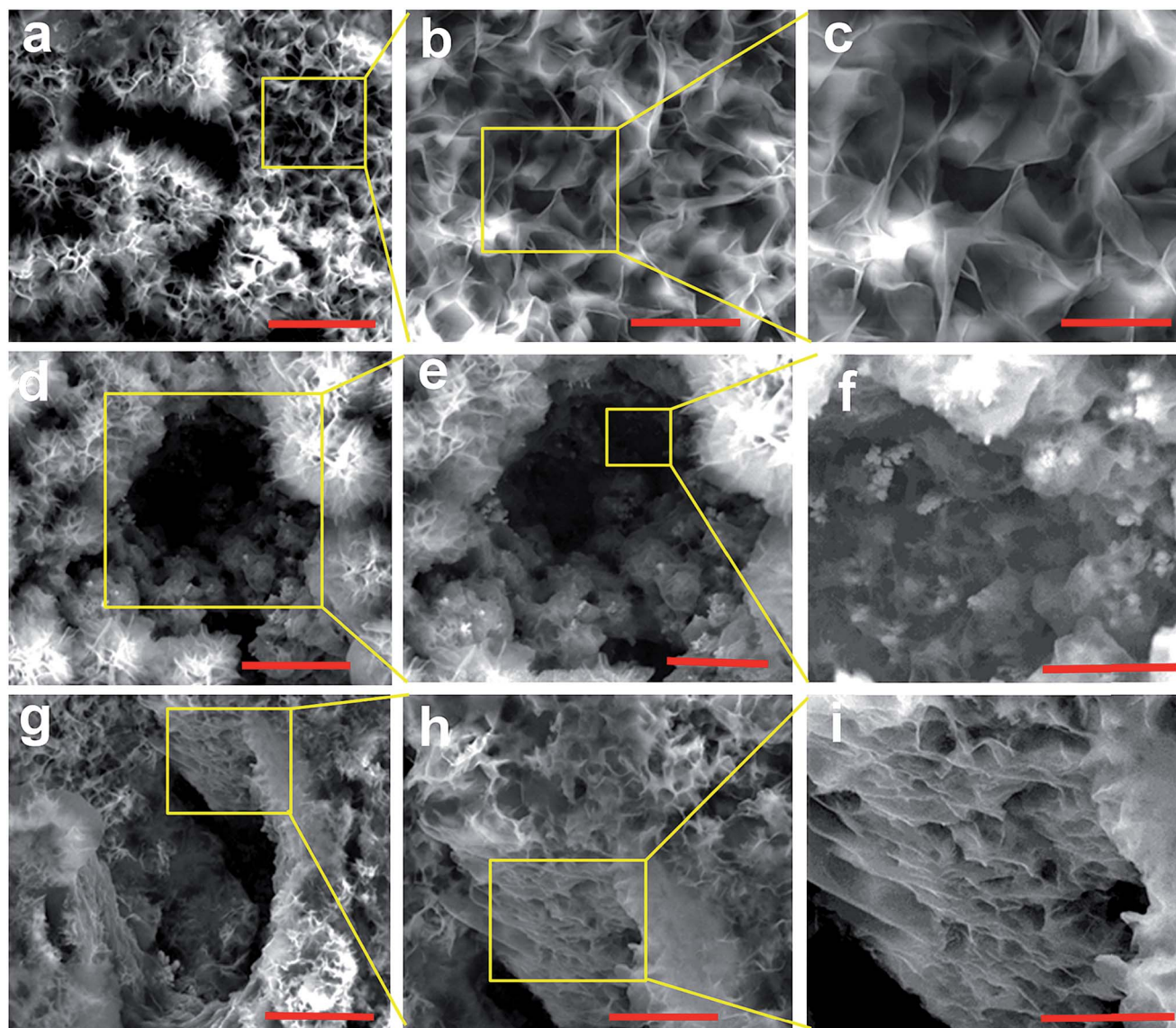
Fig. 1 Microscopic characterization of three-type structures. SEM images of (a–c) 3DrGO at the boundary of CuF, (d–f) 3DrGO inside the pore of CuF and (g–i) 3DrGO on the wall of CuF. The scale of bars: (a) 50 μm, (b) 10 μm, (c) 5 μm, (d) 50 μm, (e) 20 μm, (f) 10 μm, (g) 50 μm, (h) 20 μm and (i) 10 μm.

symmetric rectangular shape is largely retained only with a slight distortion at high scan rates. This observation suggests that 3DrGO@CuF electrodes have high capacitive performance and small internal resistance of 3DrGO at the CuF surfaces and interfaces. It is important to note that the amount of GO self-assembled on CuF and the pore size of CuF have significant impacts on the specific capacitance (C_{sp}) of 3DrGO@CuF. The voltammetric and charge–discharge behaviour of 3DrGO@CuF with different loadings of GO was evaluated (Fig. S12 ESI†). The C_{sp} was calculated from the charge–discharge curve, and it was observed that 0.08 mg cm^{-2} of GO on CuF contributes the highest specific capacitance (Table S1 ESI†). The specific capacitance decreases with increasing GO loading. The SEM micrograph (Fig. S4 ESI†) shows that increasing GO loading affects the porous structure, leading to the formation of an aggregated structure when the GO loading was larger than

0.4 mg cm^{-2}. We have also evaluated the effects of the CuF pore size on the C_{sp} of the 3DGO@CuF material. The 3DGO@CuF electrodes with different pore sizes of CuF were synthesized by changing the electrodeposition time but keeping the same loading amount of GO at 0.08 mg cm^{-2}. The CVs and charge–discharge curves were recorded with these materials (Fig. S13 ESI†). The 3DrGO@CuF electrodes with an average pore size of ≈120 μm (*i.e.* 60 s electrodeposition) give the best performance (Table S1 and Fig. S13 ESI†). This observation can be explained by the structural characteristics revealed by SEM. As shown by the SEM images (Fig. S5 ESI†), the CuF with a pore size of ≈120 μm is well covered with rGO layers to form an open porous 3D network. In addition, we have also synthesized the CuF with a thickness larger than 150 μm by increasing the electrodeposition time. However, the as-synthesized thicker CuFs are not stably retained but often detached from the Cu foil bulk.

6326 | *J. Mater. Chem. A*, 2015, **3**, 6324–6329

This journal is © The Royal Society of Chemistry 2015
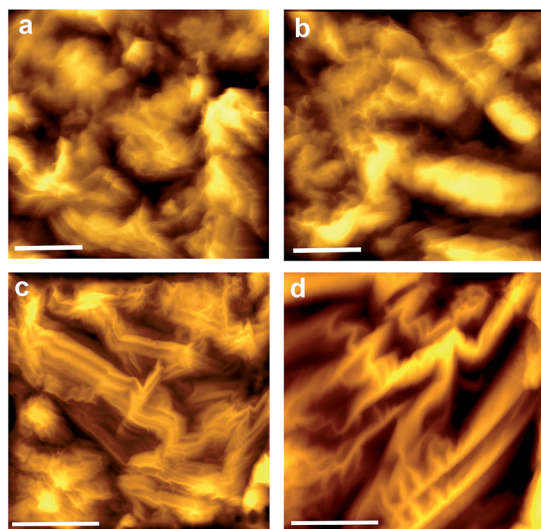
Fig. 2 High-resolution microscopic structures. AFM (a and b) images of 3DrGO–CuF on Cu supports. (c and d) are the high-resolution images. The scale of bars: (a) 5 μm, (b) 5 μm, (c) 2 μm and (d) 0.5 μm.

The capacitive performance of 3DrGO@CuF electrodes was further investigated with galvanostatic charge–discharge cycles. Fig. 3b and S14 (ESI†) show charge–discharge curves of 3DrGO@CuF electrodes at different applied current densities ranging from 1 to 100 A g^{-1}. The C_{sp} of the material was calculated from the discharging curves and is plotted *vs.* current density (Fig. 3c). The C_{sp} of 3DrGO@CuF electrodes at 1 A g^{-1} can reach 623 ± 7 F g^{-1}, which is among the highest specific capacitance reported for 3DrGO based materials.[5a,6,7,12] However, the observed capacitance is contributed not only by 3DrGO but also from CuF itself as discussed below. As expected, the C_{sp} decreases with increasing current density. However, the specific capacitance is still high even at high current densities. For instance, the material retained its C_{sp} at 416 F g^{-1} with 10 A g^{-1} applied (*i.e.* 67% retained with respect to that obtained at 1 A g^{-1}) and 317 F g^{-1} at 100 A g^{-1} (*i.e.* 51% retained). There is no *IR* drop observed at high current densities (5 to 100 A g^{-1}) on the discharge curves and very small *IR* drop observed at low current densities (1 to 2 A g^{-1}). This observation indicates that the electrodes have a small internal resistance, consistent with the conclusion from voltammetric results (Fig. 3a). In addition, one interesting feature noted is that 3DrGO@CuF electrodes show excellent cycling performance (2000 continuous cycles) even at a high current density such as 10 A g^{-1} (Fig. 3d). Symmetrical and triangular charge–discharge curves observed indicate a low mass transfer resistance and good charge propagation of electrolyte ions in the porous 3DrGO networks, which is highly desirable for an ideal supercapacitor.[13] A slight enhancement in C_{sp} is observed up to the first 500 cycles (*i.e.* from 416 increased to 430 F g^{-1}, Fig. 3e) which is likely due to initial activation of the material, and after that the capacitance remains largely constant in the following cycles. After 2000 cycles, the C_{sp} value reduced slightly to 425 F g^{-1} but with still ~99% retention of C_{sp} with respect to the steady C_{sp} (430 F g^{-1}) after 500 cycles, indicating that the electrodes possess good

cycling stability and a high degree of reversibility. Following cycling stability measurements, the system durability was checked by cyclic voltammetry. Clearly, there is no detectable decay in voltammetric responses after 2000 cycles (Fig. S15 ESI†), suggesting that the structural integrity is retained. To further confirm the structural feature after cycling, we checked the SEM images before and after cycling. It is clear from the SEM images (Fig. S16 ESI†) that the structure of the 3DGO@CuF material does not change its integrity after 2000 charge–discharge cycles.

To clarify the contributions of Cu components (including bulk Cu and Cu foam) and GO to the high specific capacitance (623 F g^{-1}) observed, the control experiments with CuF and 3DGO@CuF as supercapacitor electrodes were performed in parallel. Their CVs and charge–discharge curves were recorded and are compared to those for 3DrGO@CuF (Fig. S17 ESI†). The C_{sp} of CuF and 3DGO@CuF is 20 F g^{-1} and 234 F g^{-1}, respectively, about 30 and 3 times lower than that for 3DrGO@CuF electrodes. Therefore, 3DGO@CuF can also be used as super-capacitor electrodes, but the electrochemical conversion of GO into rGO is essential for enhancing performance in the present case. In the case of CuF alone, the initial capacitance was very small (only 20 F g^{-1}). However, we noticed that upon further charge–discharge cycling at a fixed current density (*e.g.* 1 A g^{-1}) the specific capacitance of CuF increased continuously up to 1000 cycles (Fig. S18 ESI†). The specific capacitance obtained after 1000 cycles was 110 F g^{-1}, which was stable up to 1700 cycles then decreased.

It is reported that the quantum capacitance of graphene can reach up to 21 μF cm^{-2},[14] which is equivalent to ~550 F g^{-1} by assuming that all the specific surface areas (2630 m^2 g^{-1}) were fully effectively used. As the contribution from CuF is 110 F g^{-1}, the specific capacitance contributed by 3DrGO is approximately 513 F g^{-1} *i.e.* over 90% of the theoretical value. This estimate does not cover possible cooperative contributions from the two components, rGO and Cu foam. On the other hand, the results do show that this hybrid integrated system can generate high specific capacitance arising from optimal assembly and likely synergic interactions between rGO and CuF.

Electrochemical impedance spectroscopy (EIS) was used to reveal the possible mechanisms of fast ion diffusion behaviour in conducting porous films. EIS spectra were recorded at the open circuit potentials of the systems in the frequency range of 10^5 Hz to 0.1 Hz with an amplitude of 10 mV applied and compared for different systems (Fig. S19 ESI†). The Nyquist plot of 3DrGO@CuF electrodes features a vertical curve almost parallel to the *Y*-axis (black dots in Fig. S19 ESI†), indicating fast diffusion and propagation of ions within the porous framework. In the high frequency region, the curves intersecting the real axis approximately at a 45° angle (the inset in Fig. S19 ESI†) signifies fast kinetics of ion transfer, which is an advantageous feature of a porous electrode when saturated with electrolyte.[12c]

The Ragone plot of the present system, which is a characteristic indication of both energy density and power density, is shown in Fig. 3f. The maximum energy density of 31 W h kg^{-1} is achieved with a power density of 0.3 kW kg^{-1}. The maximum power density of 30 kW kg^{-1} is obtained with an energy density

This journal is © The Royal Society of Chemistry 2015

J. Mater. Chem. A, 2015, **3**, 6324–6329 | **6327**
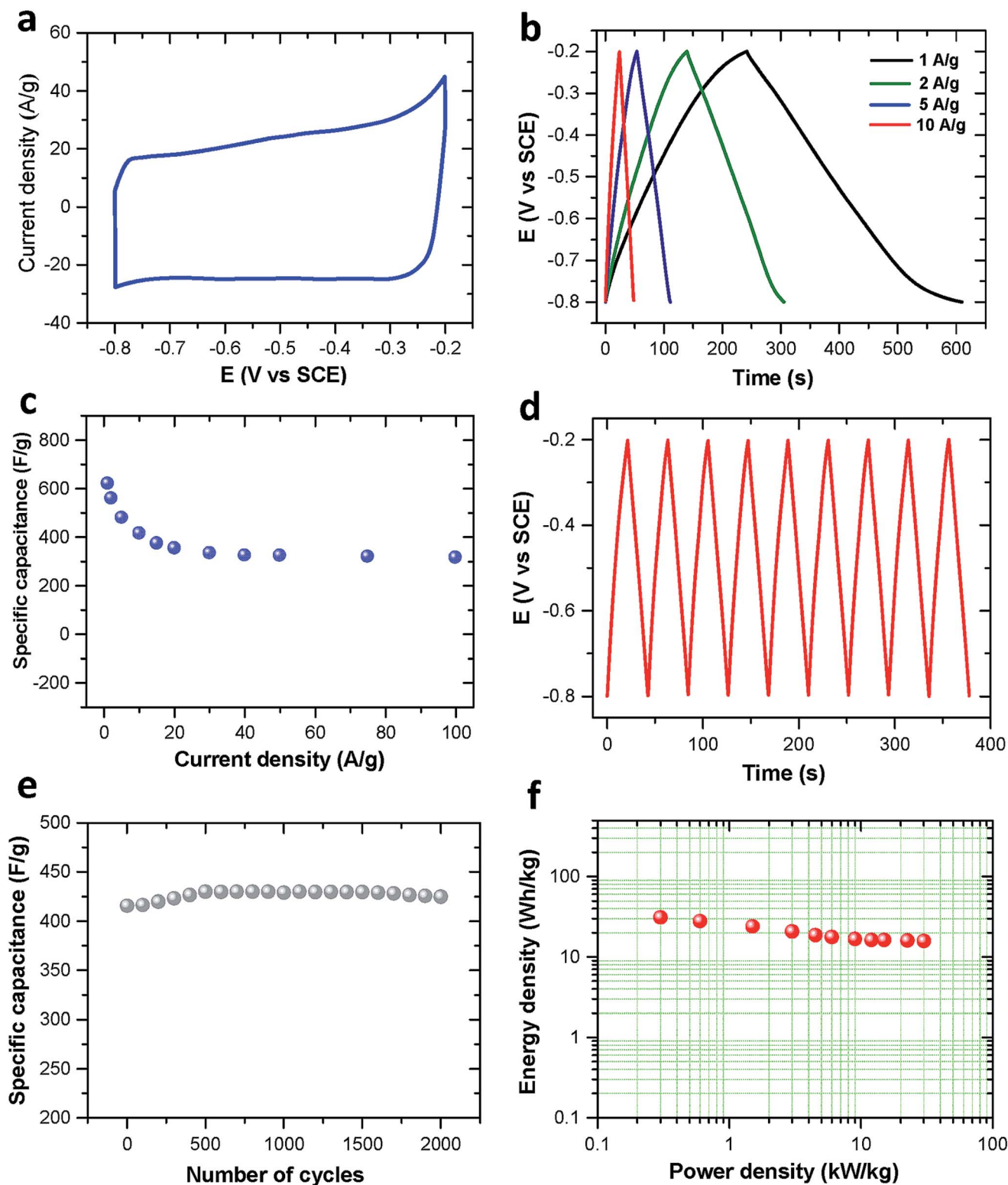
Fig. 3 Supercapacitive performance of 3DrGO@CuF electrodes in PBS. (a) Cyclic voltammogram obtained with a scan rate of 100 mV s^{-1}. (b) Comparison of charge–discharge curves obtained at different current densities. (c) Dependence of specific capacitance on applied current density. (d) Successive charge–discharge cycles at a current density of 10 A g^{-1}. (e) Change of specific capacitance over the charge–discharge cycles. (f) Typical Ragone plot for the present system.

6328 | J. Mater. Chem. A, 2015, 3, 6324–6329

This journal is © The Royal Society of Chemistry 2015

of 16 W h kg^{-1}. The energy density is significantly higher than most reported values to date for pure porous graphene-based materials in the literature.[5b,6a,12a–b]

In conclusion, Cu foam serves as an effective framework for self-assembly of three-dimensional GO networks that can be converted into rGO by electroreduction, and the Cu substrate acts as an excellent current collector. The overall procedure enables us to fabricate all-in-one supercapacitor electrodes with integrated 3DrGO networks as major capacitive species. The resulting 3DrGO@CuF electrodes have small internal resistance and exhibit high specific capacitance and cycling stability. Furthermore, the high-performance is achieved in environmentally friendly neutral solutions instead of commonly used strong acidic or basic solutions as well as with a relatively narrow potential window applied. The present system thus holds great potential to be further enhanced in supercapacitive performance, for example by extension of its potential windows in organic media or/and ionic liquids. Among others, such a detailed study is underway.

Acknowledgements

Notes and references

1 (a) Y. Sun, Q. Wu and G. Shi, *Energy Environ. Sci.*, 2011, **4**, 1113; (b) Y. Zhu, *et al.*, *Adv. Mater.*, 2010, **22**, 3906; (c) R. S. Dey, S. Hajra, R. K. Sahu, C. R. Raj and M. K. Panigrahi, *Chem. Commun.*, 2012, **48**, 1787.

2 Y. Zhu, *et al.*, *Science*, 2011, **332**, 1537.

3 H. Huang, L. Xu, Y. Tang, S. Tang and Y. Du, *Nanoscale*, 2014, **6**, 2426.

4 (a) Z.-S. Wu, D.-W. Wang, W. Ren, J. Zhao, G. Zhou, F. Li and H.-M. Cheng, *Adv. Funct. Mater.*, 2010, **20**, 3595; (b) S. Chen, J. Zhu, X. Wu, Q. Han and X. Wang, *ACS Nano*, 2010, **4**, 2822; (c) Q. Wu, Y. Xu, Z. Yao, A. Liu and G. Shi, *ACS Nano*, 2010, **4**, 1963.

5 (a) W. Wei, X. Cui, W. Chen and D. G. Ivey, *Chem. Soc. Rev.*, 2011, **40**, 1697; (b) D. Bélanger, T. Brousse and J. W. Long, *Electrochem. Soc. Interface*, 2008, **17**, 49; (c) K. Gopalakrishnan, K. Moses, A. Govindaraj and C. N. R. Rao, *Solid State Commun.*, 2013, **175–176**, 43; (d) K. Gopalakrishnan, A. Govindaraj and C. N. R. Rao, *J. Mater. Chem. A*, 2013, **1**, 7563.

6 (a) L. Zhang and G. Shi, *J. Phys. Chem. C*, 2011, **115**, 17206; (b) Y. Xu, K. Sheng, C. Li and G. Shi, *ACS Nano*, 2010, **4**, 4324; (c) S. Ye, J. Feng and P. Wu, *ACS Appl. Mater. Interfaces*, 2013, **5**, 7122; (d) L. Zhang, F. Zhang, X. Yang, G. Long, Y. Wu, T. Zhang, K. Leng, Y. Huang, Y. Ma, A. Yu and Y. Chen, *Sci. Rep.*, 2013, **3**, 1408.

7 X. Cao, Z. Yin and H. Zhang, *Energy Environ. Sci.*, 2014, **7**, 1850.

8 (a) K. Wang, X. Dong, C. Zhao, X. Qian and Y. Xu, *Electrochim. Acta*, 2015, **152**, 433; (b) X. Dong, K. Wang, C. Zhao, X. Qian, S. Chen, Z. Li, H. Liu and S. Dou, *J. Alloys Compd.*, 2014, **586**, 745; (c) C. Zhao, S.-L. Chou, Y. Wang, C. Zhou, H.-K. Liu and S.-X. Dou, *RSC Adv.*, 2013, **3**, 16597.

9 O. C. Compton, Z. An, K. W. Putz, B. J. Hong, B. G. Hauser, L. C. Brinson and S. T. Nguyen, *Carbon*, 2012, **50**, 3399.

10 S. Trasatti and O. A. Petrii, *J. Electroanal. Chem.*, 1992, **327**, 353.

11 (a) F. Liu, S. Y. Song, D. F. Xue and H. J. Zhang, *Adv. Mater.*, 2012, **24**, 1089; (b) W. F. Chen, S. R. Li, C. H. Chen and L. F. Yan, *Adv. Mater.*, 2011, **23**, 5679–5683.

12 (a) U. N. Maiti, J. Lim, K. E. Lee, W. J. Lee and S. O. Kim, *Adv. Mater.*, 2014, **26**, 615; (b) Z. Lei, F. Shi and L. Lu, *ACS Appl. Mater. Interfaces*, 2013, **5**, 9656; (c) C. M. Niu, E. K. Sichel, R. Hoch, D. Moy and H. Tennent, *Appl. Phys. Lett.*, 1997, **70**, 1480.

13 (a) J. Yan, T. Wei, B. Shao, F. Ma, Z. Fan, M. Zhang, C. Zheng, Y. Shang, W. Qian and F. Wei, *Carbon*, 1731, **2010**, 48; (b) W.-W. Liu, X.-B. Yan, J.-W. Lang, C. Peng and Q.-J. Xue, *J. Mater. Chem.*, 2012, **22**, 17245; (c) L. L. Zhang, X. Zhao, M. D. Stoller, Y. Zhu, H. Ji, S. Murali, Y. Wu, S. Perales, B. Clevenger and R. S. Ruoff, *Nano Lett.*, 2012, **12**, 1806.

14 J. Xia, F. Chen, J. Li and N. Tao, *Nat. Nanotechnol.*, 2009, **4**, 505.

This journal is © The Royal Society of Chemistry 2015

J. Mater. Chem. A, 2015, **3**, 6324–6329 | **6329**